DR HASSAN JAVED (Orcid ID : 0000-0002-4522-4038)

Article type : Special Issue Article

Design and characterization of novel glass-ceramic sealants for solid oxide electrolysis cell (SOEC) applications

Hassan Javed[1*], Antonio G. Sabato[1], Kai Herbrig[2], Domenico Ferrero[3], Christian Walter[2], Milena Salvo[1] and Federico Smeacetto[1]

[1] Department of Applied Science and Technology (DISAT), Politecnico di Torino, Italy

[2] Sunfire GmbH, Gasanstaltstraße 2, Dresden Germany

[3] Department of Energy (DENERG), Politecnico di Torino, Italy

Abstract

In this work, three new glass-ceramic compositions are designed and characterised as sealant materials for solid oxide electrolysis cells (SOEC), having operating temperature of 850°C. The crystallization and the sintering behavior of the glasses are investigated by using differential thermal analysis (DTA) and heating stage microscopy (HSM), respectively. The glasses show glass transition temperatures of 715-740°C, while the coefficients of thermal expansion (CTE) of 9.3-10.3 $\times 10^{-6}$ K^{-1}

This article has been accepted for publication and undergone full peer review but has not been through the copyediting, typesetting, pagination and proofreading process, which may lead to differences between this version and the Version of Record. Please cite this article as doi: 10.1111/ijac.12889

(200°C-500°C) are measured for the glass-ceramics, matching with the CTEs of the other cell components. The compatibility between the glass-ceramic sealants, the 3YSZ electrolyte and the Crofer22APU interconnect is examined by means of SEM and EDS, in the as-joined condition and after 1000 hours at 850°C in air. Compositional changes in the glass-ceramic sealants are reviewed and discussed with respect to the formed crystalline phases before and after the ageing treatment at 850°C.

* Corrosponiding author: hassan.javed@polito.it

Key words: Thermal expansion, SOEC, interfaces, crystals/crystallization

1. Introduction

Solid oxide electrolysis cells (SOECs) have gained special attention as a promising technology for the production of hydrogen by using electrical energy preferably obtained from various renewable energy sources (1, 2). SOEC can operate in a reverse principle as a solid oxide fuel cell (SOFC), which involves the combination of hydrogen and oxygen to generate electrical energy(3). SOEC systems mostly operate in the temperature range of 700°C-850°C, therefore the degradation of cell components can be a limiting factor for their performance (4, 5). In this context, a major challenge faced in SOEC technology is the synthesis of reliable sealants. Sealants are required for the full utilization of the potential of SOECs and to achieve maximum efficiency. Additionally, sealants are important to prevent any gas leakage through the cells and the interconnects, and to provide electrical insulation between the interconnects within a stack (6, 7). In order to work efficiently in the SOEC environment, sealants need to fulfill a variety of requirements, many of which are the same as those required for SOFC operation. For instance, the sealants should be chemically compatible and mechanically stable at high temperatures (up to 850°C); their coefficient of thermal expansion (CTE) should closely match the CTEs of the other cell components to avoid the formation

of cracks and debonding between sealants and neighboring components at a high temperature. In SOEC operation, sealants must ensure electrical insulation at higher voltage levels – typically > 1.2 V – compared to SOFC environment. The stability of sealants under thermal cycling is also a fundamental requirement, especially when SOECs are operated in reversible systems for electricity storage(8), in which the cells are alternately working as SOECs or SOFCs with different temperature profiles(9). Moreover, high pressure stability is also a peculiar requirement for sealants of SOECs operating in pressurized environments, which is a promising application showing improved cell performance at high current density(10, 11). Hence, the sealants for SOEC should be capable of working for >30,000 hours under the operating conditions of high pressure and applied thermal cycles(12-14). The sealants should also work effectively under oxidizing and reducing environment (6, 15).

Owing to the above mentioned strict requirements, the selection of the materials for sealants is not straightforward. A lot of research has been focused on glass and glass-ceramic sealants because they are rigid materials, with high mechanical strength, high electrical resistivity, high flexibility in compositions and relatively low production costs.

To achieve long term stability, special attention needs to be paid when selecting the glass composition. Several glass compositions have been used and reported in literature(6, 13-19) for SOFCs and SOECs. Alkali and alkaline earth metallic oxides are commonly used as modifiers in glasses. Alkali metal oxides (Na_2O and K_2O) reduce the viscosity, improve the wettability and enhance the CTE of glass, however, they are not the best choice due to their high chemical reactivity and low electrical resistivity(7, 20-22). Among alkaline earth metals oxides, barium oxide (BaO) has been intensively used in the past(14, 23-30). The addition of BaO increases the CTE and reduces the glass transition temperature, but has various disadvantages, i.e. it reacts with Cr present in the steel interconnect and forms barium chromate, a high CTE phase that can cause delamination at the sealant/interconnect interface due to stress generation (31). Secondly, in a glass-ceramic it can form

the celsian phase ($BaAl_2Si_2O_8$); this phase has a low CTE (2.29 x 10^{-6} K^{-1}) and can lead to the formation of thermal stresses during operation(27). Due to the above mentioned issues, it was necessary to find another alternative to BaO. Therefore, in the last few years, a trend has been shifted to use SrO as a modifier instead of BaO. The addition of SrO reduces viscosity and adjusts the CTE (20, 32-35). López et al.(36) studied and compared the mechanical properties within the BaO/SrO-MgO-B_2O_3-SiO_2 systems before and after ageing at 800°C up to 800 hours. The SrO containing composition yielded higher mechanical properties than BaO containing composition. Anyway glass-ceramic-based sealants were not evaluated in contact with the metallic interconnect. Hao et al.(37) investigated various glass systems with different modifiers and found that the SrO containing glasses had better wettability on Crofer22APU. On the other hand, the presence of a high concentration of boron oxide (B_2O_3) in glass based sealants leads to a reduction of the high temperature mechanical integrity of the sealant because of lower melting point of B_2O_3(38). Additionally, at a high working temperature of SOEC, the volatilization of B_2O_3 increases the sealant porosity, thus causing gas leakage. The volatile species of B_2O_3 can also contaminate the anode and effect its performance (39).

Most of the glass compositions available in literature have been mainly studied for the working temperature of 800 °C (1, 6, 13, 15, 36, 38, 40, 41). Few compositions have been studied up to the working temperature of 850 °C (31, 42). For instance, Mahapatra et al. (42) demonstrated that the SrO–La_2O_3–Al_2O_3–SiO_2 (SABS-0) glass system was stable at 850°C for at least 200 hours. Nevertheless, Chou et al.(28) examined electrical properties of the SrO based glass (YS046) for 500-1000 hours at 800-850°C and found the formation of unwanted Sr chromates at glass/Crofer22APU interface after 500 hours of operation. Similarly another SrO based glass composition (YS075) (43) was studied mainly focusing on the tensile strength degradation of sealing glass-ceramic/metallic interconnect interfaces with and without aluminizing processes on the interconnect. The formation of $SrCrO_4$ resulted in crack formation at glass/Crofer22APU interface, while the aluminization of the metallic

interconnect surface was found to be a viable method to prevent adverse chromates formation, as studied up to 300 hours at 850 °C.

Reddy et al.(44) studied new series of developed lanthanide containing diopside glass-ceramic sealants with SrO content in the 7-12 mol% range. The proposed glass-ceramics had excellent properties after joining, nevertheless all the reported glass-ceramics showed reduction in their CTEs during thermal ageing from 500 hours to 1000 hours. Moreover, the compatibility of these glass-ceramics with a Sanergy HT metallic interconnect and an 8YSZ solid electrolyte were discussed up to 500 hours.

This study provides a new insight into Ba free glass sealants for SOECs applications, for the working temperature of 850 °C. SrO was used as the main glass modifier in addition to CaO and MgO, and the concentration of B_2O_3 was limited to a maximum of 6 ml%. SrO was preferred over BaO due to the fact that Ba tends to react with Cr more readily than Sr to form a chromate compound, though both chromate formation reactions are thermodynamically favorable with negative Gibbs free energies(45). The durability of these new sealants was studied at 850°C for 1000 hours in static air.

The main objective of this paper is to compare 3 new glass-based compositions with different amounts of SrO as a modifier, by reviewing its effect on crystal phases formation as well as on thermal and thermomechanical properties of the glass-ceramic sealant in contact with a Crofer22APU interconnect @ 850°C.

2. Experimental

Three glasses were synthesized by thoroughly mixing different oxides and carbonates. The raw materials used for the preparation of the glasses were SiO_2 (>99%), H_3BO_3 (99.99%), $CaCO_3$ (>99%), $MgCO_3$ (>99.5%), $SrCO_3$ (>99%), Al_2O_3 (99.9%) and Y_2O_3 (99.99%). The glass compositions are reported in Table 1 and are labeled as HJ1, HJ3 and HJ4. The glass compositions were designed by using the

SciGlass® database (Science Serve GmbH, SciGlass 6.6 software, Newton, MA, USA). All the reported glass compositions are free from alkali metal oxides. HJ1 glass has CaO and MgO as main modifiers. In addition to that a minimal amount of SrO was also added. In HJ3 system the concentrations of SiO_2 and SrO were increased, as compared with HJ1, at the partial expenses of CaO and MgO. However, in HJ4, CaO and MgO were completely omitted to further increase the concentration of SrO. Other components such as B_2O_3, Al_2O_3 and/or Y_2O_3 has been added to all compositions to adjust the viscosity.

For glass synthesis, the mixture of the raw materials (oxides and carbonates) was melted at 1600 °C in a platinum crucible for 1 hour. The melted mixture was then air quenched on a brass plate. The synthesized glasses were then crushed using ball milling and sieved to obtain glass particles < 25 µm.

The glasses were characterized by differential thermal analysis (DTA Netzsch, Eos, Selb, Germany) up to 1300°C at a heating rate of 5°C/min, to analyze their characteristic temperatures. The sintering behavior of glasses was observed by heating stage microscopy (HSM Expert system solutions, Modena Italy) up to 1300°C at a heating rate of 5°C/min. The coefficient of thermal expansion (CTE) of the as-cast glass, glass-ceramics and glass-ceramics aged for 1000 hours at 850 °C was measured by using a dilatometer (Netzsch, DIL 402 PC/4) at a heating rate of 5 °C/min. The dilatometry was performed on the cylindrical samples with a diameter of 4 mm and height of 5 mm. For dilatometry measurements, the samples of glass were prepared by metallographic polishing the as-cast glass to obtain the above mentioned dimensions, however for glass-ceramics, the glass powder was pressed to form a cylindrical pellet, followed by heat treatment. For DTA, HSM and dilatometry analysis, three scans were made for each glass composition. The crystalline phase analysis of the glass-ceramics before and after thermal ageing was carried out by using PanAlytical X'Pert Pro PW 3040/60 Philips (The Netherlands), with Cu K_α and the X'Pert software. The XRD analysis were carried out in the range of 2 theta 10° - 70°, with step size of 0.02626° and time per step 10.20 sec.

The compatibility of glass-ceramics sealants with the Crofer22APU interconnect and 3YSZ electrolyte was investigated by SEM (Merlin ZEISS). For SOEC applications, 8YSZ is commonly used as electrolyte due to its high ionic conductivity(8). However, in this study 3YSZ is used, because it is typically used in the electrolyte supported cells thanks to its superior toughness as compared with 8YSZ(46, 47). To investigate the compatibility, the Crofer22APU/Glass/3YSZ joined samples were processed in a Carbolite furnace (CWF 13/5) in static air. Prior to the joining, each substrate, with dimensions of 1.5 cm x 1.5 cm, was cleaned with acetone. The glass was then deposited by spatula in the form of slurry containing the glass powder and ethanol in 70:30 wt%. During the joining procedure a load of 15 g/cm^2 was placed on the samples. The joining of the HJ1 and HJ3 sealants was done at 950 ^{o}C for 1 hour at a heating rate of 5 ^{o}C/min. However, for the HJ4 sealant the joining was carried out at 950°C for the dwelling time of 5 hours, at a heating rate of 2 ^{o}C/min. Further details about the selection of the different joining cycles are given in section 3.1.

The cross sections of Crofer22APU/glass-ceramics/3YSZ joined samples were metallographically polished up to 1 μm by diamond paste and investigated by SEM after coated with gold.

3. Results

3.1. Thermal Analysis

The DTA curves corresponding to the three glass systems and their shrinkage behavior vs temperature, obtained from HSM, are shown in Figure 1. In Figure 1(a), the T_g, T_x and T_p labels corresponds to glass transition temperature, onset crystallization temperature and peak crystallization temperature, respectively. The average characteristic temperatures (of three measurements) along with their standard deviations are summarized in Table 2.

Form the data in Figure 1(a), it is apparent that the DTA thermogram of HJ1 glass system showed sharp exothermic peaks of crystallization, while the intensity of the crystallization peak reduced

significantly in HJ3 glass. However, no crystallization peak was observed during the DTA analysis of the HJ4 glass system. Also, the HSM curves of the glasses (Figure 1(b)) indicate a clear difference in the sintering behavior of the different sealants. The T_{FS} (temperature of first shrinkage), reported in Figure 1(b), corresponds to the temperature at which the sintering process was initiated by viscous flow, whereas T_{MS} corresponds to the maximum shrinkage temperature.

The comparative study of HJ1 and HJ3 systems showed that by increasing the mass concentration of SrO in HJ3, a higher CTE of as-cast glass was measured as compared with the HJ1 system. Whereas, the as-cast HJ4 glass showed lowest value of CTE. On the other hand, the HJ3 and HJ4 glasses showed the glass transition (T_g) shifted to a higher temperature in spite of having a higher SrO concentration.

The glass-ceramics derived from the different parent glass compositions were obtained with the heat treatments mentioned in section 2. From the data obtained from DTA and HSM (Table 2), the heat treatment of 950 ^{o}C, 1h at a heating rate of 5 °C/min, was chosen to ensure maximum devitrification for all glasses. The CTEs of the obtained glass-ceramics for HJ1 and HJ3 systems, increased significantly as compared with their as-cast glasses. However, this heat treatment caused negligible increase in CTE of HJ4 glass-ceramic as compared with as-cast glass, probably due to a slight devitrification. Therefore, to ensure sufficient devitrification, the slow heating rate of 2^{o}C/min and long dwelling time of 5 hours was chosen as a heat treatment to prepare HJ4 glass-ceramic (as it will be shown in Figure 4). After suitable heat treatments, the CTEs of all the glass-ceramics, given in Table 2, were within the desired range (9-12 x 10^{-6} K^{-1}), taking into consideration the CTEs of the other cell components (CTEs for Crofer22APU and 3YSZ are 12 x 10^{-6} K^{-1} and 10.5 x 10^{-6} K^{-1} respectively) (48).

The CTEs measured after ageing the glass-ceramics for 1000 hours at 850°C are also reported in Table 2. The CTEs of the HJ1 glass-ceramics were slightly reduced after ageing. For the HJ3 glass-ceramic no change in the CTE was observed. On the other hand, thermal ageing slightly increased the CTE of the HJ4 glass-ceramic.

3.2. XRD and microstructural analysis

The XRD of as-cast glasses for three different glass systems is shown in figure S1. The XRD patterns of the different glass-ceramics before and after ageing are shown in Figure 2. As-joined HJ1 glass-ceramic, in Figure 2(a), showed the formation of Anorthite ($CaAl_2Si_2O_8$) as the main crystalline phase; in addition, Akermanite-gehlenite $Ca_2(Mg_{0.5}Al_{0.5})(Si_{1.5}Al_{0.5}O_7)$ was also present as the secondary phase. In HJ3 glass-ceramic, Figure 2(b), $Sr_2Al_2SiO_7$ was found to be the main crystalline phase, with Sr-diopside ($Ca_{0.75}Sr_{0.2}Mg_{1.05}(Si_2O_6)$ and Akermanite ($Ca_2MgSi_2O_7$) as secondary phases. Figure 2(c) shows the XRD patterns of the HJ4 system treated at different temperatures and for different dwelling times (Table 2). The HJ4 glass-ceramic treated at 950°C for 1 hour, contained only $SrSiO_3$ as the crystalline phase in addition to the residual glassy phase. However, an increase in the dwelling time to five hours at 950°C, resulted in the formation of cristobalite (SiO_2) as secondary phase in addition to $SrSiO_3$ as main phase. The XRD patterns of HJ1, HJ3 and HJ4 glass-ceramics after ageing at 850 °C, 1000 hours are also shown in figure 2(a), 2(b) and 2(c) respectively. The XRD patterns of pure phases shown in figure 2, corresponds to the simulated patters obtained from the X'Pert software data base. The different crystalline phases present in as-joined and aged glass-ceramics are summarized in Table 3.

The SEM cross-section images of the interfaces of the HJ1, HJ3 and HJ4 glass-ceramics with Crofer22APU and 3YSZ substrates are shown in Figure 3. The evolution of microstructure of the HJ4 system after processing at different heat treatments along with corresponding EDS analysis, is

shown in Figure 4. The heat treatment of 950°C, 1h (Figure 4(a)) shows that a significant amount of residual glassy phase was still present (dark area). Only one type of crystalline phase was observed. On the other hand, the heat treatment at 950°C, 5h at 2°C/min resulted in the formation of a new phase.

Figure 6 shows the Crofer22APU/glass-ceramic interface for the HJ1, HJ3 and HJ4 systems after thermal ageing for 1000 hours at 850^{o}C. The EDS line scans across the Crofer22APU/HJ1-, Crofer22APU/HJ3- and the Crofer22APU/HJ4-interface are shown in Figure 7 .

4. Discussion

In HJ1 composition CaO and MgO were added as the main modifiers. The SrO addition was minimal (9% mol) in HJ1 with the main purpose to act as a network modifier. SrO concentration was increased in HJ3 and further in HJ4 to have Sr containing crystalline phases in addition to having minimal SrO in the residual glass phase, thus maintaining a viscous glass behavior and to reduce the potential formation of Sr chromate. A proper balance of SiO_2/SrO (equal to 1) is required to obtain a desired high CTE $SrSiO_3$ phase (10.9 x 10^{-6} K^{-1}) (49), however as the increasing of SrO contents also increases the possibility of formation of undesirable $SrCrO_4$ phase, improving one property could potentially come at the expenses of other functionalities, and the right balance is often difficult to achieve. Therefore, the SiO_2/SrO in HJ3 and HJ4 was kept 2.3 and 1.99 respectively, slightly higher than some glasses reported in literature (28, 43) where formation of $SrCrO_4$ resulted in poor adhesion of glass-ceramic with interconnects. To this purpose, the proposed glass compositions require high silica contents in order to obtain high viscosities and desired crystalline phases, considering the high operating temperatures of the SOECs at 850°C and the potential reactivity of the Crofer22APU with SrO.

4.1. Thermal Analysis

The difference in the crystallization behavior of different glasses, obtained from DTA (Figure 1(a)), indicate that the intensity of crystallization reduced from HJ1 to HJ4. In HJ4 glass, probably the crystallization was not enough to be detected during the DTA analysis. The HSM analysis of the HJ1 and HJ3 systems (Figure 1(b)), which have more devitrification than HJ4, showed a constant shrinkage for a certain temperature range after the completion of sintering (T_{MS}). On the contrary, HJ4, showed a continuous viscous flow at temperatures higher than the $T_{FS,}$ due to the fact of having low devitrification.

In order to obtain dense and consequently, leakage free sealants, it is necessary to complete the sintering before the crystallization starts ($T_{MS} < T_x$), thus avoiding the formation of porosity in the sealant due to increased viscosity caused by crystal growth(7). As soon as the crystallization occurs, the glass viscosity will drastically increase, hindering the viscous flow of the glass and the adhesion to the metallic or ceramic substrates. Therefore, the crystallization mechanism of the glass-ceramic should be controlled and taken into account in the heat treatment schedule. In the HJ1 and HJ3 glass systems the sintering was completed prior to the beginning of the crystallization (Table 2).

Addition of modifiers reduce the characteristic temperatures and improves the CTE of glasses due to increase in number of non-bridging oxygen atoms. This effect becomes more prominent with increasing atomic radii of modifiers used(23). The HJ3 and HJ4 glass system resulted in high *Tg* values as compared with HJ1 in spite of high SrO concentration. Wang et al.(50) also found higher glass transition temperatures when the amount of SrO increased, but no explanation was provided for this. According to Yiannopoulos et al. (51) the addition of alkaline earth metals oxides to boron containing glasses causes an increase in T_g up to a certain concentration. However, a further increase in concentration results in the reduction of T_g. Following this hypothesis, increasing concentration up to a certain level adds additional bridging oxygen atoms to the SiO^{-4} unit cell and increases the rigidity of the network and consequently the T_g. A further addition of alkaline earth metals oxides

leads to the formation of non-bridging oxygen atoms and thus causes the breakage of the network and reduces the T_g.

On the other hand, HJ3 as-cast glass showed higher CTE as compared with HJ1 due to having high SrO concentration. However, the HJ4 as-cast glass showed lowest CTE among all glass systems in spite of having high concentration of SrO as compared with HJ3. The reduction in CTE of as-cast HJ4 glass is due to reducing the overall concentration of the modifiers.

The obtained glass-ceramics after heat treatment showed higher CTEs then parent glasses due to phase transformation. Due to the more intensity of crystallization in HJ1 and HJ3 glass systems, the heat treatment at 950 °C, 1h at a heating rate of 5 °C/min was enough to improve the CTE of their respective glass-ceramics for SOEC applications. However, this heat treatment did not improve the CTE of HJ4 glass-ceramic probably due to the less devitrification in HJ4 system. Therefore, the HJ4 glass-ceramics obtained at slow heating rate and at long dwelling time showed the maximum increase in CTE from its parent glass, due to the increase in the amount of high CTE $SrSiO_3$ phase.

Ageing of glass-ceramics at 850 °C for 1000h reduced the CTEs of HJ1 glass-ceramic (Table 2). It was likely due to the presence of the $CaAl_2Si_2O_8$ phase as detected by XRD (Figure 2(a)), having a CTE of 4.9 x 10^{-6} K^{-1} (52). For the HJ3 glass-ceramic no change in the CTE was observed in spite of having a low CTE $Sr_2Al_2Si_2O_7$ phase (Figure 2(a)), with CTE of 1.1 x 10^{-6} K^{-1} (53). The presence of a high CTE Sr-diopside phase(44) was responsible for retaining the overall CTE of the HJ3 glass-ceramic. On the other hand, thermal ageing slightly increased the CTE of the HJ4 glass-ceramic. This increase was probably due to an increase in the quantity of the $SrSiO_3$ phase having CTE of 10.9 x 10^{-6} K^{-1} (49) .

4.2. XRD and microstructural analysis

The XRD of as-cast glasses (Figure S1) showed an amorphous hump without any sharp crystalline peak, thus confirmed their amorphous structure. The XRD patterns of HJ1 glass-ceramic (Figure 2(a)),

showed the formation of Anorthite ($CaAl_2Si_2O_8$) as main phase while solid solution of Akermanite-Gehlenite $Ca_2(Mg_{0.5}Al_{0.5})(Si_{1.5}Al_{0.5}O_7)$ as secondary phase. The $CaAl_2SiO_8$ phase has CTE of 4.9 x 10^{-6} K^{-1} (52), and $Ca_2(Mg_{0.5}Al_{0.5})(Si_{1.5}Al_{0.5}O_7)$ has CTE around 7.7-8.0 x 10^{-6} K^{-1} (54). No Sr containing phase was detected in HJ1 due to its minimal concentration (9 mol%), thus indicating that the SrO was only present in the residual glassy phase. The HJ3 and HJ4 systems with higher SrO concentration formed Sr containing crystalline phases. In HJ4 glass-ceramic, the higher SrO content and a suitable SiO_2/SrO resulted in the formation of desired $SrSiO_3$. The long dwelling time (5h) resulted in the devitrification of secondary SiO_2 phase (cristobalite) in addition to $SrSiO_3$. The presence of cristobalite could be an issue in particular if the joined samples would have been submitted to thermal cycles, since a phase transformation around 270°C (with a change in the specific volume) can lead thermomechanical stresses in the microstructure with possible crack formation, thus affecting the joined structure integrity.

The XRD of the aged glass-ceramics of HJ1, HJ3 and HJ4 systems as shown in Figure 2(a), 2(b) and 2(c) respectively, indicate that these systems were stable after ageing and no new phase was formed.

The SEM analysis of Crofer22APU/ as-joined glass-ceramic interfaces (Figure 3) show continuous interfaces, thus confirming a strong adhesion of the three glass-ceramics with both the Crofer22APU and 3YSZ substrates. There was no evidence of any cracks, gaps or delamination at both interfaces. The microstructure of the glass-ceramics was dense (low fractions of pores) and uniform throughout the sample.

The detail examination of the Crofer22APU/HJ1 interface (Figures 3(a)) clearly showed a continuous thin layer of crystals as indicated by the white arrow. The growth of these crystals (1-2 µm) was most likely due to the heterogeneous nucleation where the Crofer22APU substrate served as the nucleation site. No strontium chromate was detected at the Crofer22APU/HJ1 interface (at least after the joining process in air atmosphere).

The microstructure of the HJ3 glass-ceramic (Figure 3(c) and 3(d)) showed the presence of different types of crystalline phase in addition to the residual glassy phase. Figures 3(e) and 3(f) also show a very dense HJ4-based joint with little porosity, as well as its strong adhesion with both of the joined materials. The "viscous character" of this system led to a negligible level of porosity during the joining treatment.

The microstructure of the HJ4 system after processing at different heat treatments is shown in Figure 4. The microstructure of HJ4 glass-ceramic obtained after the heat treatment of 950°C, 1h (Figure 4(a)) shows the presence of only one crystalline phase in addition to the residual glass phase. According to XRD (Figure 2(b)) that phase corresponds to $SrSiO_3$. On the other hand, the heat treatment at 950°C, 5h at 2°C/min resulted in the significant evolution of microstructure. Apparently this heat treatment not only increased the volume fraction of the initially formed $SrSiO_3$ phase but also resulted in the devitrification of secondary SiO_2 phase (Figure 4(b)). The corresponding EDS spectrum of the dark zones in the SEM images of the HJ4 glass-ceramic microstructure indicated a SiO_2 rich phase (spot 1), whereas spot 2 showed a Si and Sr rich phase, referring to $SrSiO_3$ as investigated by XRD. EDS analysis of spot 3 was similar to spot 2, thus indicates $SrSiO_3$ phase. The different contrast between spot 2 and spot 3 was probably due to the presence of very thin glass layer on the crystals at spot 3. These EDS results validate the XRD analysis of HJ4 at different heat treatments, as discussed in section earlier.

The table 4 shows the EDS point analysis carried out at the residual glassy phases on HJ1, HJ3 and HJ4 as-joined glass-ceramics. In all the glass systems, the concentration of Sr was less than 10 at %, which was beneficial in order to maintain the viscous behavior of glassy phase. These results also rationalize the purpose behind increasing the SrO contents from HJ1 to HJ4 i-e to form SrO containing crystalline phases and to have minimal SrO in the glassy phase thus avoiding the potential formation of $SrCrO_4$. The EDS line scans across Crofer22APU/ glass-ceramics interface (Figure 5) also

confirmed that there was no formation of chromates at interface, nor diffusion of elements from either side of interface.

The Crofer22APU/glass-ceramic interface for the HJ1, HJ3 and HJ4 systems (Figure 6) investigated after the thermal ageing for 1000 hours at 850^{o}C showed a uniform and crack free microstructure. The microstructures of these glass systems were dense and similar to their as-joined microstructures (Figure 3). A good sinter-crystallization behavior of these systems, studied previously, is further confirmed, since no pores are detected in the microstructure.

The EDS line scans across the Crofer22APU/HJ1, Crofer22APU/HJ3 and the Crofer22APU/HJ4 interfaces after thermal ageing has shown in Figure 7. From the EDS line scan across Crofer22APU/HJ1 interface, the diffusion of Cr into the HJ1 glass ceramic was detected. Although, the crystalline phases in HJ1 reduced the CTE of the obtained glass-ceramic; therefore, HJ1 is the least promising sealing candidate among three studied glass systems. Nevertheless, the HJ1 glass system showed good adhesion with Crofer22APU even after aging for 1000 hours at 850°C, however, the diffusion of Cr can potentially form $SrCrO_4$ and can be critical in long terms. Moreover, presence of Cr can also alter the CTE of the glass. On the other hand, no Cr diffusion was detected in HJ3 and HJ4 glass-ceramics. These SEM results excluded the formation of $SrCrO_4$ and the consequent delamination at the Crofer22APU/glass-ceramic interface, thus making these systems as promising candidates for solid oxide cells seals at the working T of 850°C. The presence of low CTE $Sr_2Al_2SiO_7$ phase in HJ3 and cristobalite phase (with different polymorphs) (7) in HJ4 did not determine cracks within the glass-ceramics or at the interface with Crofer22APU even after 1000 hours at 850 °C.

5. Conclusions

New glass-ceramics were designed for their application as sealants for SOEC having a working temperature of 850 °C. The effect of the SrO content on the properties of novel glass sealants was investigated. The new compositions showed a difference in terms of their crystallization and sintering behavior. The thermal properties obtained, in terms of glass transition, the sequence of crystallization and sintering temperatures, were found to be suitable to obtain dense glass-ceramic sealants for the working temperature of 850 °C. For all three glass systems, the coefficient of thermal expansions of the as-joined glass-ceramics were measured as 9.3-10.3 x 10^{-6} K^{-1} which are suitable for SOEC applications and close matching with Crofer22APU and 3YSZ. However, the thermal ageing reduced the CTE of the HJ1 system due to the presence of a low CTE crystalline phase. For HJ4 composition it was found that a balanced SiO_2-SrO ratio in the glass was appropriate to produce SrSiO3 (a high CTE phase) as the main crystalline phase. For the HJ3 and HJ4 systems good compatibility and excellent interfacial bonding was observed for the glass-ceramics with the Crofer22APU and 3YSZ electrolyte before and after ageing. These characterizations showed that the investigated compositions can be promising candidates for use as sealants in Solid Oxide Electrolysis Cells at 850 °C.

6. Acknowledgments

The project leading to this research has received funding from:

-The European Union's Horizon 2020 research and innovation programme under the Marie Skłodowska-Curie grant agreement No 642557 (CoACH-ETN)".

-The Fuel Cells and Hydrogen 2 Joint Undertaking under grant agreement No 700300 (GrInHy, Green Industrial Hydrogen via reversible high-temperature electrolysis). This Joint Undertaking receives

support from the European Union's Horizon 2020 research and innovation programme and Hydrogen Europe and N.ERGHY

7. References

1. Li Q, Zheng Y, Guan W, Jin L, Xu C, Wang WG. Achieving high-efficiency hydrogen production using planar solid-oxide electrolysis stacks. International Journal of Hydrogen Energy. 2014;39(21):10833-42.

2. Kazempoor P, Braun RJ. Hydrogen and synthetic fuel production using high temperature solid oxide electrolysis cells (SOECs). International Journal of Hydrogen Energy. 2015;40(9):3599-612.

3. Mahapatra MK, Lu K. Glass-based seals for solid oxide fuel and electrolyzer cells - A review. Materials Science and Engineering R: Reports. 2010;67(5-6):65-85.

4. Hauch a, Ebbesen SD, Jensen SH, Mogensen M. Solid Oxide Electrolysis Cells: Microstructure and Degradation of the Ni/Yttria-Stabilized Zirconia Electrode. Journal of The Electrochemical Society. 2008;155(11):B1184-B.

5. Mahata A, Datta P, Basu RN. Microstructural and chemical changes after high temperature electrolysis in solid oxide electrolysis cell. Journal of Alloys and Compounds. 2015;627:244-50.

6. Khedim H, Nonnet H, Méar FO. Development and characterization of glass-ceramic sealants in the (CaO-Al 2O 3-SiO 2-B 2O 3) system for Solid Oxide Electrolyzer Cells. Journal of Power Sources. 2012;216:227-36.

7. Fergus JW. Sealants for solid oxide fuel cells. Journal of Power Sources. 2005;147(1-2):46-57.

8. Suciu C, Tikkanen H, Wærnhus I, Goga F, Dorolti E. Water-based tape-casting of SOFC composite 3YSZ/8YSZ electrolytes and ionic conductivity of their pellets. Ceramics International. 2012 2012/01/01/;38(1):357-65.

9. D. Ferrero AL, P. Leone, and M. Santarelli, editor Dynamic reversible SOC applications: Performance and Durability with simulated load/demand profiles. 11th European SOFC and SOE Forum 2014.

10. Bernadet L, Gousseau G, Chatroux A, Laurencin J, Mauvy F, Reytier M. Assessment of Pressure Effects on High Temperature Steam Electrolysis Based on Solid Oxide Technology. ECS Transactions. 2015;68(1):3369-78.

11. Kazempoor P, Wendel C, Braun RJ. Pressurized Regenerative Solid Oxide Cells for Electrical Energy Storage. ECS Transactions. 2014;58(37):45-54.

12. Kim SD, Seo DW, Dorai AK, Woo SK. The effect of gas compositions on the performance and durability of solid oxide electrolysis cells. International Journal of Hydrogen Energy. 2013;38(16):6569-76.

13. Kim SJ, Kim KJ, Choi GM. A novel solid oxide electrolysis cell (SOEC) to separate anodic from cathodic polarization under high electrolysis current. International Journal of Hydrogen Energy. 2015;40(30):9032-8.

14. Peng L, Zhu Q. Thermal cycle stability of BaO-B2O3-SiO2 sealing glass. Journal of Power Sources. 2009;194(2):880-5.

15. Sabato AG, Cempura G, Montinaro D, Chrysanthou A, Salvo M, Bernardo E, et al. Glass-ceramic sealant for solid oxide fuel cells application: Characterization and performance in dual atmosphere. Journal of Power Sources. 2016;328(October):262-70.

16. Zhang X, O'Brien JE, O'Brien RC, Hartvigsen JJ, Tao G, Housley GK. Improved durability of SOEC stacks for high temperature electrolysis. International Journal of Hydrogen Energy. 2013;38(1):20-8.

17. Smeacetto F, De Miranda A, Chrysanthou A, Bernardo E, Secco M, Bindi M, et al. Novel glass-ceramic composition as sealant for SOFCs. Journal of the American Ceramic Society. 2014;97(12):3835-42.

18. Smeacetto F, Salvo M, Santarelli M, Leone P, Ortigoza-Villalba GA, Lanzini A, et al. Performance of a glass-ceramic sealant in a SOFC short stack. International Journal of Hydrogen Energy. 2013;38(1):588-96.

19. Reddy AA, Tulyaganov DU, Goel A, Pascual MJ, Kharton VV, Tsipis EV, et al. Diopside - Mg orthosilicate and diopside - Ba disilicate glass-ceramics for sealing applications in SOFC: Sintering and chemical interactions studies. International Journal of Hydrogen Energy. 2012;37(17):12528-39.

20. Kaur B, Singh K, Pandey OP. Microstructural study of Crofer 22 APU-glass interface for SOFC application. International Journal of Hydrogen Energy. 2012;37(4):3839-47.

21. Zhu Q, Peng L, Zhang T, Chou Y-SS, Stevenson JW, Choi J-P, et al. Alkali Effect on the Electrical Stability of a Solid Oxide Fuel Cell Sealing Glass. Fuel Cell Electronics Packaging. 2010;93(3):618-23.

22. Chou Y-S, Stevenson JW, Choi J-P. Alkali Effect on the Electrical Stability of a Solid Oxide Fuel Cell Sealing Glass. Journal of The Electrochemical Society. 2010;157(3):B348-B53.

23. Tulyaganov DU, Reddy AA, Kharton VV, Ferreira JMF. Aluminosilicate-based sealants for SOFCs and other electrochemical applications - A brief review. Journal of Power Sources. 2013;242:486-502.

24. Kerstan M, Mueller M, Ruessel C. Binary, ternary and quaternary silicates of CaO, BaO and ZnO in high thermal expansion seals for solid oxide fuel cells studied by high-temperature X-ray diffraction (HT-XRD). Materials Research Bulletin. 2011;46(12):2456-63.

25. Lin SE, Cheng YR, Wei WCJ. BaO–B2O3–SiO2–Al2O3 sealing glass for intermediate temperature solid oxide fuel cell. Journal of Non-Crystalline Solids. 2012;358(2):174-81.

26. Reddy AA, Tulyaganov DU, Pascual MJ, Kharton VV, Tsipis EV, Kolotygin VA, et al. Diopside-Ba disilicate glass-ceramic sealants for SOFCs: Enhanced adhesion and thermal stability by Sr for Ca substitution. International Journal of Hydrogen Energy. 2013;38(7):3073-86.

27. Sohn S-B, Choi S-Y, Kim G-H, Song H-S, Kim G-D. Suitable Glass-Ceramic Sealant for Planar Solid-Oxide Fuel Cells. Journal of the American Ceramic Society. 2004;87(2):254-60.

28. Chou YS, Stevenson JW, Xia GG, Yang ZG. Electrical stability of a novel sealing glass with (Mn,Co)-spinel coated Crofer22APU in a simulated SOFC dual environment. Journal of Power Sources. 2010;195(17):5666-73.

29. Kerstan M, Rüssel C. Barium silicates as high thermal expansion seals for solid oxide fuel cells studied by high-temperature X-ray diffraction (HT-XRD). Journal of Power Sources. 2011;196(18):7578-84.

30. Gupta HC, Luthra V. Effects ofM2+ (M = Ca, Sr, and Ba) Addition on Crystallization andMicrostructure of SiO2-MgO-Al2O3-B2O3-K2O-F Glass. Vibrational Spectroscopy. 2011;56(2):235-40.

31. Reddy AA, Goel A, Tulyaganov DU, Kapoor S, Pradeesh K, Pascual MJ, et al. Study of calcium-magnesium-aluminum-silicate (CMAS) glass and glass-ceramic sealant for solid oxide fuel cells. Journal of Power Sources. 2013;231:203-12.

32. Ojha PK, Chongdar TK, Gokhale NM, Kulkarni AR. Investigation of crystallization kinetic of SrO-La2O3-Al2O3eB2O3-SiO2 glass and its suitability for SOFC sealant. International Journal of Hydrogen Energy. 2011;36(22):14996-5001.

33. Chou YS, Stevenson JW, Choi JP. Long-term evaluation of solid oxide fuel cell candidate materials in a 3-cell generic short stack fixture, Part II: Sealing glass stability, microstructure and interfacial reactions. Journal of Power Sources. 2014;250:166-73.

34. Reddy AA, Tulyaganov DU, Pascual MJ, Kharton VV, Tsipis EV, Kolotygin VA, et al. SrO-Containing Diopside Glass–Ceramic Sealants for Solid Oxide Fuel Cells: Mechanical Reliability and Thermal Shock Resistance. Fuel Cells. 2013;13(5):689-94.

35. Tiwari B, Dixit A, Kothiyal GP. Study of glasses/glass-ceramics in the SrO–ZnO–SiO2 system as high temperature sealant for SOFC applications. International Journal of Hydrogen Energy. 2011 2011/11/01/;36(22):15002-8.

36. Rodríguez-López S, Wei J, Laurenti KC, Mathias I, Justo VM, Serbena FC, et al. Mechanical properties of solid oxide fuel cell glass-ceramic sealants in the system BaO/SrO-MgO-B2O3-SiO2. Journal of the European Ceramic Society. 2017 2017/09/01/;37(11):3579-94.

37. Hao J, Zan Q, Ai D, Ma J, Changsheng D, Xu J. Structure and high temperature physical properties of glass seal materials in solid oxide electrolysis cell. Journal of Power Sources. 2012;214:5-83.

38. Jin T, Lu K. Thermal stability of a new solid oxide fuel/electrolyzer cell seal glass. Journal of Power Sources. 2010;195(1):195-203.

39. Sasaki K, Haga K, Yoshizumi T, Minematsu D, Yuki E, Liu R, et al. Chemical durability of Solid Oxide Fuel Cells: Influence of impurities on long-term performance. Journal of Power Sources. 2011;196(22):9130-40.

40. Chen J, Yang H, Chadeyron R, Tang D, Zhang T. Tuning the interfacial reaction between CaO–SrO–Al2O3–B2O3–SiO2 sealing glass–ceramics and Cr-containing interconnect: Crystalline structure vs. glass structure. Journal of the European Ceramic Society. 2014 2014/08/01/;34(8):1989-96.

41. Zhang T, Brow RK, Fahrenholtz WG, Reis ST. Chromate formation at the interface between a solid oxide fuel cell sealing glass and interconnect alloy. Journal of Power Sources. 2012 2012/05/01/;205(Supplement C):301-6.

42. Mahapatra MK, Lu K, Bodnar RJ. Network structure and thermal property of a novel high temperature seal glass. Applied Physics A. 2009;95(2):493-500.

43. Chou Y-S, Stevenson JW, Singh P. Effect of aluminizing of Cr-containing ferritic alloys on the seal strength of a novel high-temperature solid oxide fuel cell sealing glass. Journal of Power Sources. 2008 2008/12/01/;185(2):1001-8.

44. Reddy AA, Goel A, Tulyaganov DU, Sardo M, Mafra L, Pascual MJ, et al. Thermal and mechanical stability of lanthanide-containing glass-ceramic sealants for solid oxide fuel cells. Journal of Materials Chemistry A. 2014;2(6):1834-46.

45. Chou Y-S, Stevenson JW, Singh P. Novel Refractory Alkaline Earth Silicate Sealing Glasses for Planar Solid Oxide Fuel Cells. Journal of The Electrochemical Society. 2007;154(7):B644-B51.

46. Badwal SPS. Zirconia-based solid electrolytes: microstructure, stability and ionic conductivity. Solid State Ionics. 1992;52(1):23-32.

47. Kondoh J, Shiota H, Kawachi K, Nakatani T. Yttria concentration dependence of tensile strength in yttria-stabilized zirconia. Journal of Alloys and Compounds. 2004;365(1):253-8.

48. Ghosh S, Das Sharma A, Kundu P, Basu RN. Glass-ceramic sealants for planar IT-SOFC: A bilayered approach for joining electrolyte and metallic interconnect. Journal of the Electrochemical Society. 2008;155(5):B473-B8.

49. Thieme C, Rüssel C. Thermal expansion behavior of SrSiO3 and Sr2SiO4 determined by high-temperature X-ray diffraction and dilatometry. Journal of Materials Science. 2015;50(16):5533-9.

50. Wang X, Ou DR, Zhao Z, Cheng M. Stability of SrO–La2O3–Al2O3–SiO2 glass sealants in high-temperature air and steam. Ceramics International. 2016;42(6):7514-23.

51. Yiannopoulos YD, Chryssikos GD, Kamitsos EI. Structure and properties of alkaline earth borate glasses. Phys Chem Glasses. 2001;42(May 2001):164-72.

52. Cheng X, Ke S, Wang Q, Wang H, Shui A, Liu P. Fabrication and characterization of anorthite-based ceramic using mineral raw materials. Ceramics International. 2012 2012/05/01/;38(4):3227-35.

53. Manu KM, Ananthakumar S, Sebastian MT. Electrical and thermal properties of low permittivity Sr2Al2SiO7 ceramic filled HDPE composites. Ceramics International. 2013 2013/07/01/;39(5):4945-51.

54. Merlini M, Gemmi M, Artioli G. Thermal expansion and phase transitions in åkermanite and gehlenite. Physics and Chemistry of Minerals. 2005 June 01;32(3):189-96.

List of figures:

Table 1. Composition of glass sealants (mol%)

	SiO_2	B_2O_3	CaO	MgO	SrO	Al_2O_3	Y_2O_3
HJ1	36.73	4.53	16.87	23.47	9.13	9.27	---
HJ3	47.07	3.69	11.45	12.74	19.85	3.78	1.42
HJ4	57.6	5.65	---	---	28.84	6.17	1.74

Table 2. Characteristic temperatures of different glasses (Heating rate: 5°C/min)

	HJ1	HJ3	HJ4		
Glass transition temperature T_g (°C)	715 ± 3	722 ± 3	736 ± 4		
Onset crystallization temperature T_x (°C)	905 ± 5	893 ± 5	Not detected		
Peak crystallization temperature T_p (°C)	922 ± 2	936 ± 2	Not detected		
First shrinkage temperature T_{FS} (°C)	778 ± 3	773 ± 3	809 ± 5		
Maximum shrinkage temperature T_{MS} (°C)	840 ± 4	855 ± 2	875 ± 4		
CTE of as-cast glass/1 x 10^{-6} K (200 °C-500 °C)	8.2 ± 0.1	9.7 ± 0.2	6.9 ± 0.1		
CTE of as-joined glass-ceramic/1 x 10^{-6} K (200 °C-500 °C)	9.6[a] ± 0.2	10.2[a] ± 0.2	7.0[a] ± 0.1	8.2[b] ± 0.2	9.3[c] ± 0.1
CTE of glass-ceramic aged for 1000 h at 850 °C (200 °C-500 °C) 1 x 10^{-6} K^{-1}	8.8 ± 0.3	10.1 ± 0.2	9.6[c] ± 0.1		

Heat treatment a: Room Temperature-950 °C (1 h), Heating/cooling rate 5 °C/min

b: Room Temperature-950 °C (5 h), Heating/cooling rate 5 °C/min

c: Room Temperature-950 °C (5 h), Heating/cooling rate 2 °C/min

Table 3. Crystalline phases (and relative ICCD reference number cards) present in different as-joined and aged glass-ceramics (1000h, 850 °C), as detected by XRD

	As-joined glass-ceramic	**Aged glass-ceramic**
HJ1	**$CaAl_2Si_2O_8$** (# 00-041-1486) **$Ca_2(Mg_{0.5}Al_{0.5})(Si_{1.5}Al_{0.5}O_7)$** (# 01-079-2423)	**$CaAl_2Si_2O_8$** (# 00-041-1486) **$Ca_2(Mg_{0.5}Al_{0.5})(Si_{1.5}Al_{0.5}O_7)$** (# 01-079-2423)
HJ3	**$Sr_2Al_2SiO_7$** (# 01-075-1234) **$Ca_{0.75}Sr_{0.2}Mg_{1.05}(Si_2O_6)$** (# 01-080-0388) **$Ca_2Mg(Si_2O_7)$** (# 01-083-1815)	**$Sr_2Al_2SiO_7$** (# 01-075-1234) **$Ca_{0.75}Sr_{0.2}Mg_{1.05}(Si_2O_6)$** (# 01-080-0388) **$Ca_2Mg(Si_2O_7)$** (# 01-083-1815)
HJ4	**$SrSiO_3$** (# 01-087-0474)	**$SrSiO_3$** (# 01-087-0474) **SiO_2** (# 01-082-0512)

Table 4. The EDS point analysis (at.%) at the residual glassy phase of as-joined HJ1, HJ3 and HJ4 glass-ceramics

Elements	HJ1	HJ3	HJ4
O	67.6	66.3	72.3
Mg	2.8	5.2	---
Al	8.0	1.4	2.8
Si	13.1	14.2	16.4
Ca	5.2	2.9	---
Sr	3.3	9.4	7.1
Y	---	0.6	1.4

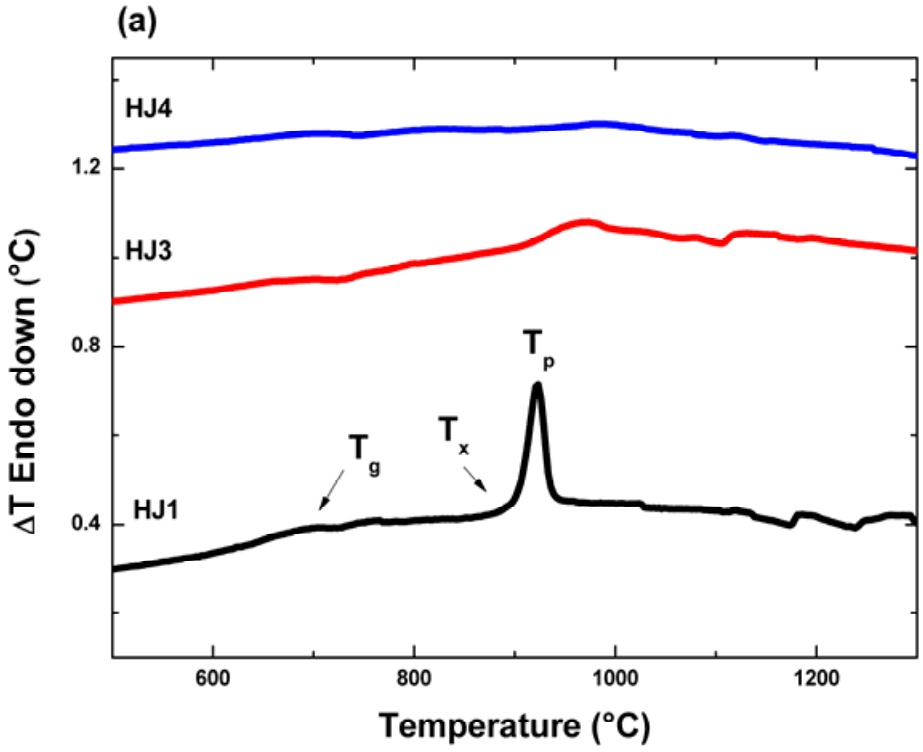

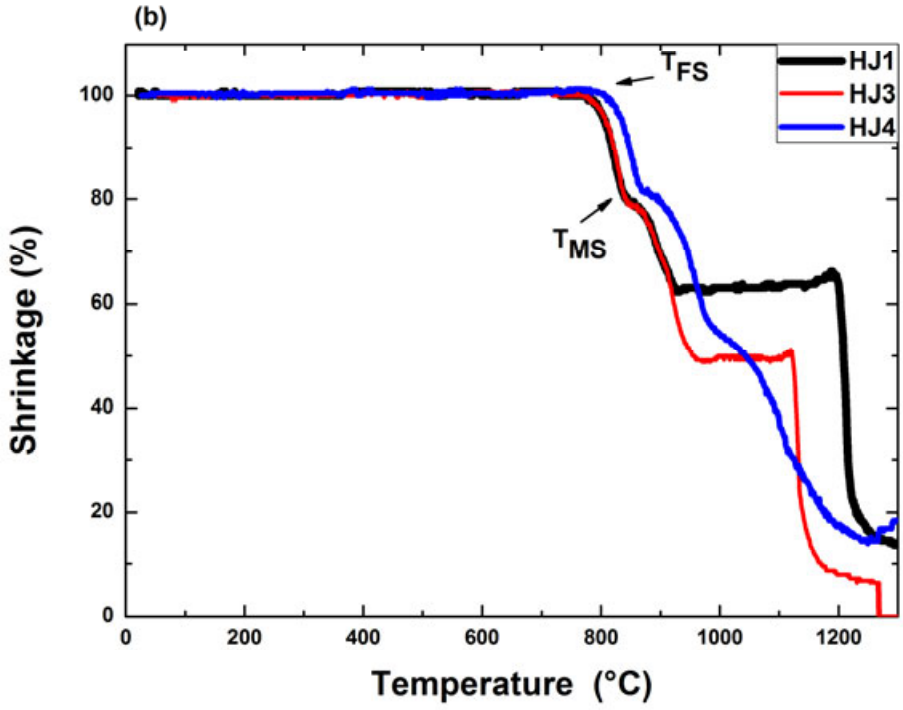

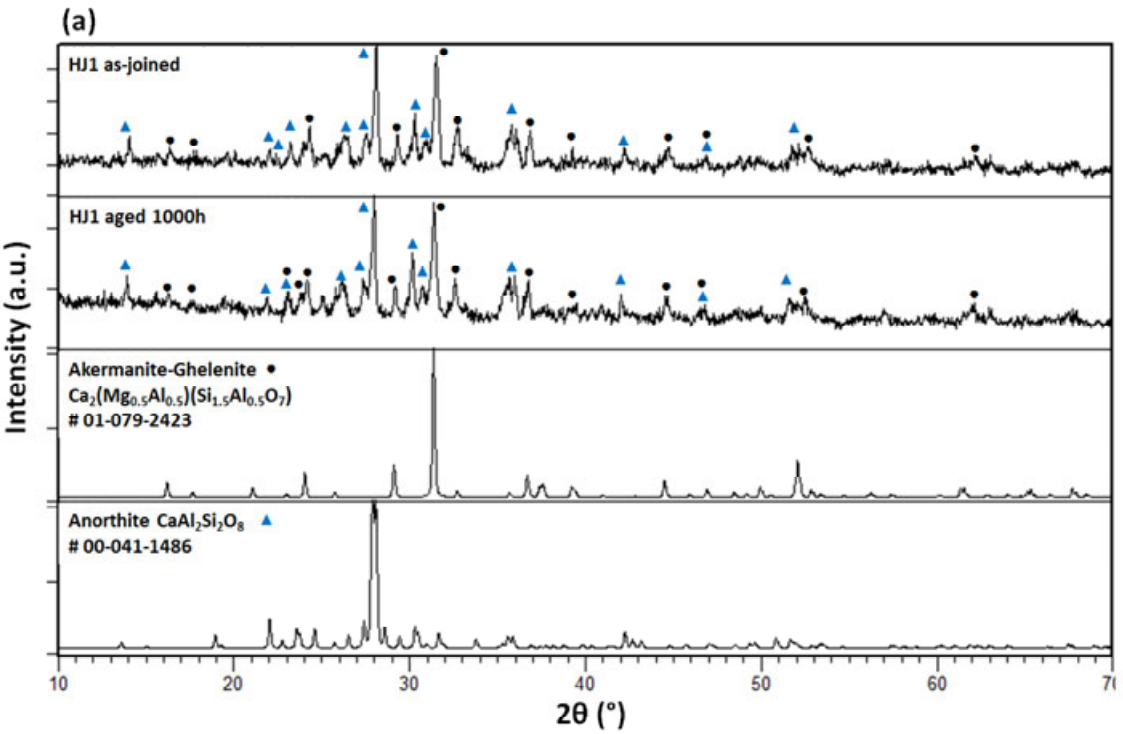

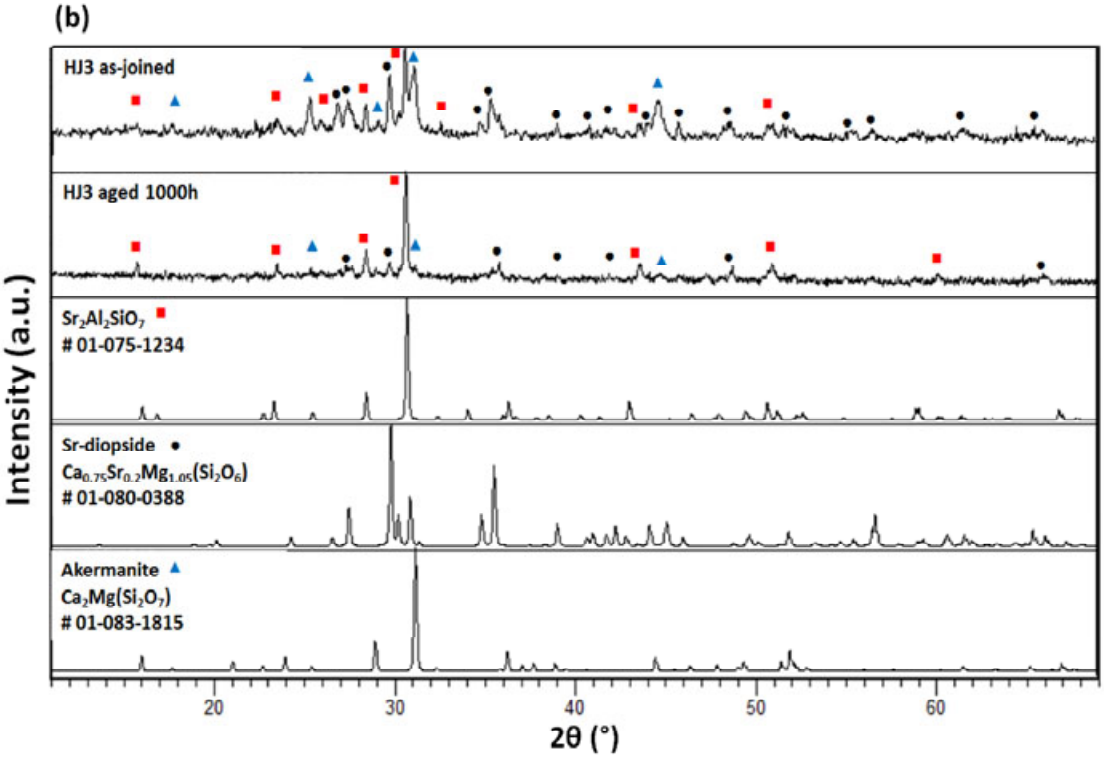

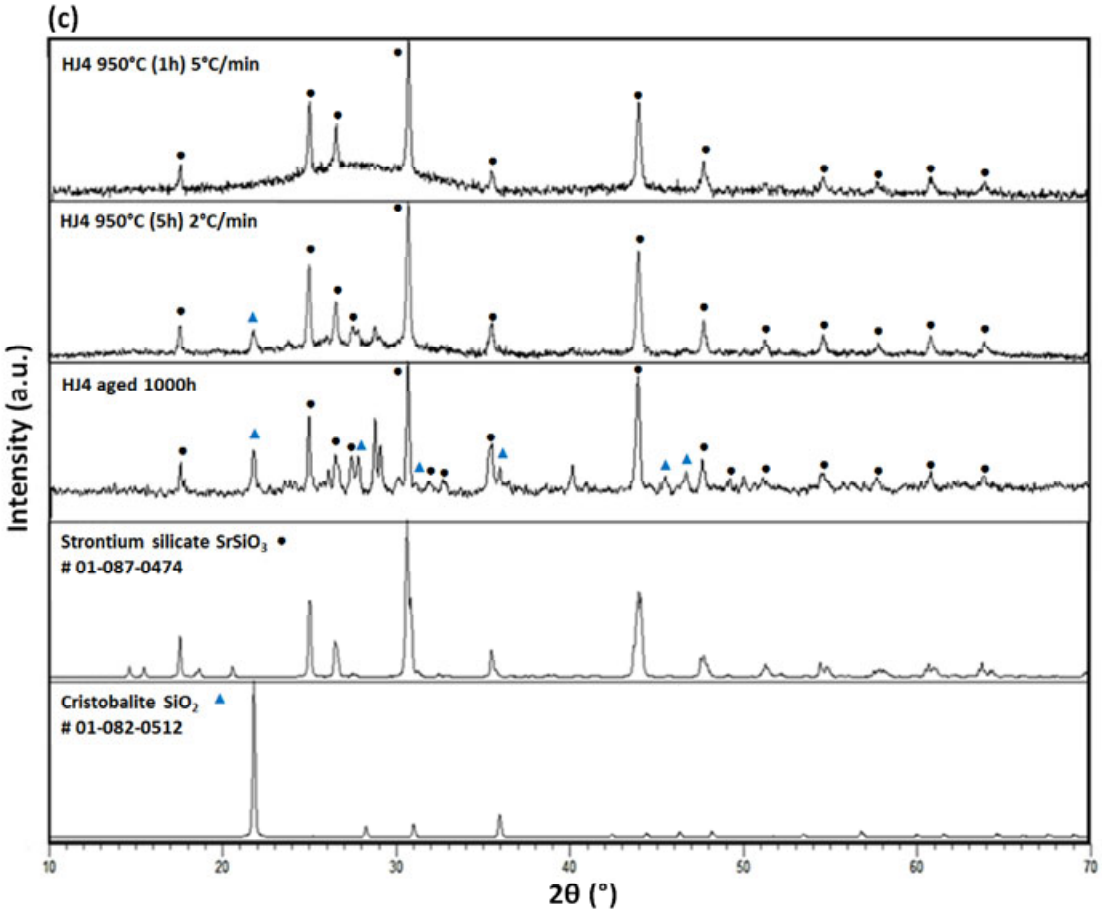

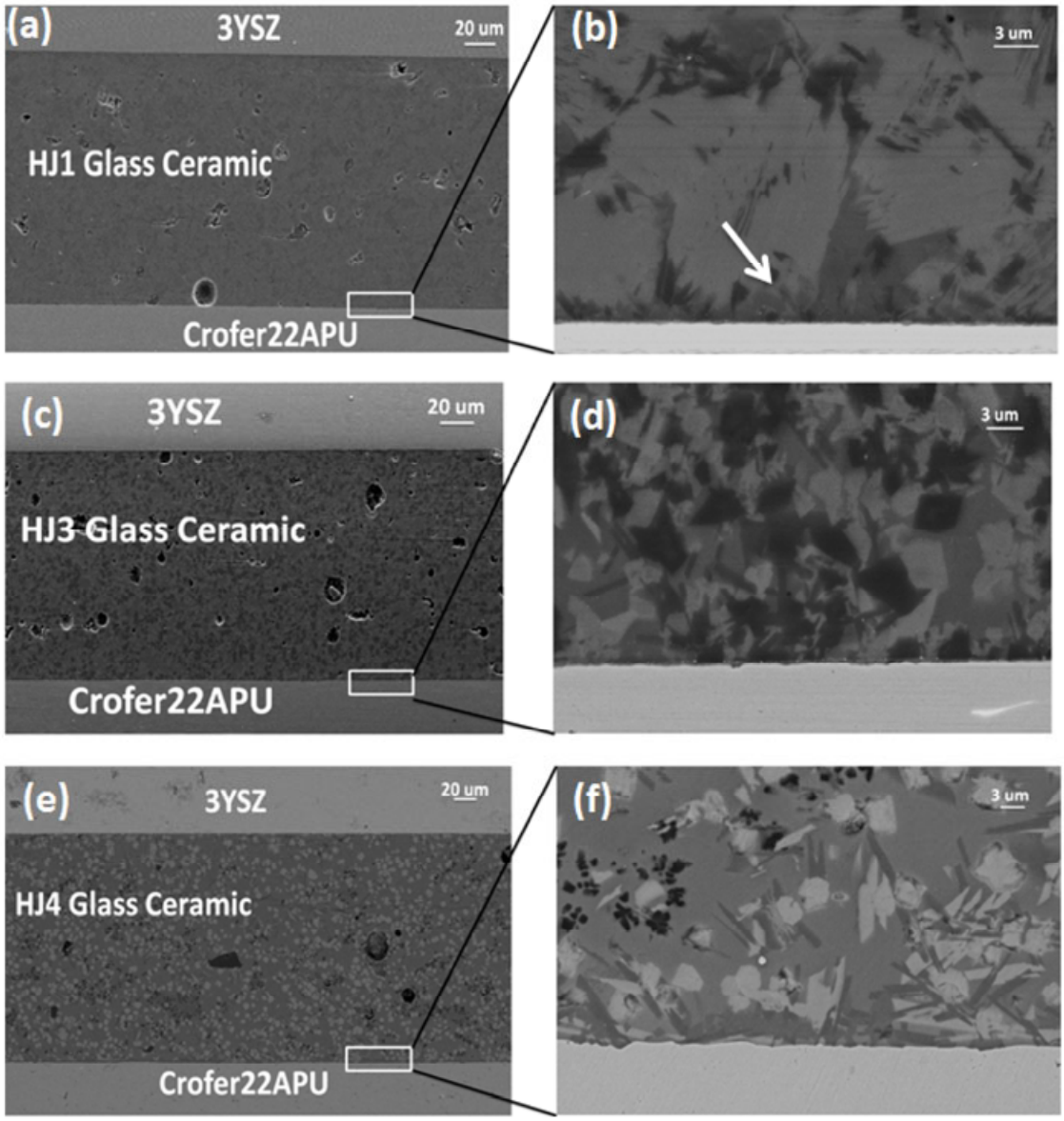

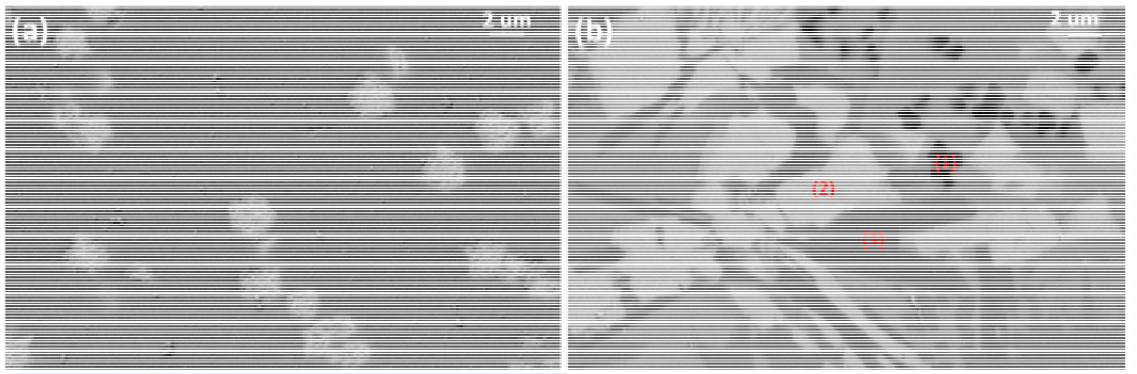

Element	Atomic %		
	1	2	3
O	74.3	68.6	75.1
Al	3.8	0.4	1.3
Si	16.4	15.6	17.3
Sr	5.5	14.9	6.4
Y	0.0	0.5	0.0